

Exploring the Higgs Sector of a Most Natural NMSSM and its Prediction on Higgs Pair Production at the LHC

Junjie Cao^{1,2}, Dongwei Li^{1,3}, Liangliang Shang^{1,4}, Peiwen Wu⁴ and Yang Zhang⁴

¹ *Department of Physics, Henan Normal University, Xinxiang 453007, China*

² *Center for High Energy Physics, Peking University, Beijing 100871, China*

³ *Department of Foundation, Henan Police College, Zhengzhou 450000, China*

⁴ *State Key Laboratory of Theoretical Physics,
Institute of Theoretical Physics, Academia Sinica, Beijing 100190, China*

Abstract

As a most natural realization of the Next-to Minimal Supersymmetry Standard Model (NMSSM), λ -SUSY is parameterized by a large λ around one and a low $\tan\beta$ below 10. In this work, we first scan the parameter space of λ -SUSY by considering various experimental constraints, especially the limitation from the Higgs data updated by the ATLAS and CMS collaborations in the summer of 2014, then we study the properties of the Higgs bosons. We get two characteristic features of λ -SUSY in experimentally allowed parameter space. One is the triple self coupling of the SM-like Higgs boson may get enhanced by a factor over 10 in comparison with its SM prediction. The other is the pair production of the SM-like Higgs boson at the LHC may be two orders larger than its SM prediction. All these features seem to be unachievable in the Minimal Supersymmetric Standard Model and in the NMSSM with a low λ . Moreover, we also find that naturalness plays an important role in selecting the parameter space of λ -SUSY, and that the Higgs χ^2 obtained with the latest data is usually significantly smaller than before due to the more consistency of the two collaboration measurements.

PACS numbers: 14.80.Da, 12.60.Jv

I. INTRODUCTION

Compared with the situation in 2012, the existence of a new scalar with mass around 125GeV has been further corroborated by the ATLAS and CMS collaborations with a local statistical significance reaching 9σ and more than 7σ respectively[1–4]. Especially, recently both the collaborations updated their measurements on the properties of the scalar by using the detector calibration in the event reconstruction[5–8], and as indicated by their published data, the two group measurements now agree with each other in a much better way. So far the mass of the scalar is rather precisely determined, and its other properties, albeit still with large experimental uncertainties, coincide with those of the Higgs boson predicted by the Standard Model (SM). Nevertheless, the issue of whether this particle is the SM Higgs boson is still open, and indeed there are some motivations, such as the gauge hierarchy problem and the intriguing slight excess of the di-photon signal for the scalar over the SM prediction, which now is $\mu_{\gamma\gamma} = 1.17 \pm 0.27$ by the ATLAS measurement[5] and $\mu_{\gamma\gamma} = 1.13 \pm 0.24$ by the CMS measurement[8], to consider new physics interpretation of this particle. Studies in this direction have been performed intensively in supersymmetric theories (SUSY)[9, 10], which are considered as the most promising new physics candidates due to their capability to unify the gauge couplings, provide a viable Dark Matter candidate as well as stabilize the weak scale in a much better way than the SM. These studies indicated that, although in the Minimal Supersymmetric Standard Model (MSSM) there exists a broad parameter space to fit the Higgs data quite well[11, 12], the mass of the observed particle leads to a well-known tension with naturalness since it is much larger than the upper bound of the tree-level Higgs mass, which is controlled by the weak gauge coupling due to the structure of the model[13]. This tension led to a revival of interest in non-minimal realizations of SUSY at the weak scale. Arguably the simplest among such extended constructions is the Next-to-Minimal Supersymmetric Standard Model (NMSSM)[14], which will be the focus of this paper.

In the NMSSM, the particle content is extended by including a gauge singlet superfield \hat{S} with its interaction with the MSSM Higgs superfields \hat{H}_u and \hat{H}_d taking the form $\lambda\hat{S}\hat{H}_u\cdot\hat{H}_d$ ($\hat{H}_u\cdot\hat{H}_d \equiv \epsilon_{ab}\hat{H}_u^a\hat{H}_d^b$ is $SU(2)$ index contraction)[14]. The inclusion of the singlet allows the quartic terms of the Higgs potential to get a new contribution, which is proportional to λ^2 . This will lift the tree-level Higgs mass and consequently alleviate the tension[13]. In fact, it is due to this advantage that the NMSSM was widely adopted to interpret the LHC

results[10]. While on the other hand, since λ is up bounded by the perturbativity of the theory below the grand unification scale, i.e. $\lambda \leq 0.7$, the size of the lift is mild and so the naturalness problem is only partially addressed. Under such a situation, λ -SUSY which corresponds to the NMSSM with a relatively large λ around 1 was recently emphasized[15–17]. As suggested by the pioneer works in this direction, the NMSSM may still maintain the grand unification and perturbativity for such a λ if an appropriate new dynamics is implemented at a certain ultraviolet energy scale[18, 19]. Moreover, it was pointed out that in λ -SUSY, the sensitivity of the weak scale to the scalar top quark (stop) mass is reduced by a factor of $\sim (g/\lambda)^2$ in comparison with the MSSM (g is the SM weak gauge coupling), which means that the lower bound on the stop mass imposed by the LHC direct searches has a weaker implication on fine-tuning in this model than in the MSSM or the NMSSM with a low λ [19]. In this sense, λ -SUSY has been treated as a most natural realization of SUSY at weak scale.

In λ -SUSY, the phenomenology in Higgs sector is rather special. Firstly, since the tree-level mass of the SM-like Higgs boson (denoted by h hereafter) may be easily higher than 125GeV, the boson must have sizable singlet and/or non-SM doublet components. Consequently, its couplings might deviate significantly from their SM predictions which will be constrained by the recently updated Higgs data[16, 17]. Secondly, unlike the MSSM where a large $\tan\beta$ is preferred to enhance the tree-level Higgs mass, $\tan\beta$ in λ -SUSY must be rather low, i.e. $\tan\beta \lesssim 4$, to coincide with the electro-weak precision data[19, 20]. In this case, the constraints of the LHC direct search for neutral non-SM Higgs bosons by $\tau\bar{\tau}$ channel are weakened[22], and the non-SM Higgs bosons may be significantly lighter than those of the MSSM. This will result in a rather different phenomenology[21], but so far is paid little attention in literature. Thirdly, as we mentioned before, the quartic terms of the Higgs potential are altered greatly in λ -SUSY so that the interactions among the physical Higgs particles may be significantly strengthened[16]. Under such a situation, the hh production may be greatly enhanced by the mediation of the non-SM Higgs bosons, which may decay into the Higgs pair dominantly[23], and/or by the trilinear self coupling of the SM-like Higgs boson, which may be much stronger than the SM prediction in some parameter region of the λ -SUSY. Considering the importance of the pair production in extracting the Higgs self coupling information, such enhancement effects should be investigated carefully. Noting above features, we in this work first consider various experimental constraints on λ -SUSY, then we

explore the Higgs sector by focusing on the properties of the lightest and the next-to-lightest CP-even Higgs bosons. We also investigate how large the Higgs pair production rate may get enhanced in λ -SUSY.

This work is organized as follows. In Sec. II, we recapitulate the framework of λ -SUSY and the features of its Higgs sector. Then we scan its parameter space by considering various constraints to get physical parameter points. In Sec. III, we investigate the predictions of these points on the properties of the lightest and the next-to-lightest CP-even Higgs boson, such as their couplings and decay rates, to show their distinctive features. In Sec. IV, we study the SM-like Higgs pair production process, and point out that its rate in λ -SUSY may be enhanced by a factor of 100 over its SM prediction, which is hardly achieved in the MSSM. Finally, we draw our conclusions.

II. HIGGS SECTOR IN λ -SUSY AND OUR SCAN STRATEGY

A. Higgs Sector in NMSSM with a Large λ

The NMSSM extends the MSSM with one gauge singlet superfield \hat{S} , and since it aims at solving the μ problem of the MSSM, a Z_3 discrete symmetry under which the Higgs superfields \hat{H}_u , \hat{H}_d and \hat{S} are charged is implemented in the construction of the superpotential to avoid the appearance of parameters with mass dimension. As a result, its superpotential is given by [14]

$$W^{\text{NMSSM}} = W_F + \lambda \hat{H}_u \cdot \hat{H}_d \hat{S} + \frac{1}{3} \kappa \hat{S}^3, \quad (1)$$

where W_F is the superpotential of the MSSM without the μ -term, and λ, κ are all dimensionless parameters describing the interactions among the superfields. The scalar potential for the Higgs fields H_u , H_d and S is given by the sum of the usual F- and D-term contributions, and the soft breaking terms:

$$V_{\text{soft}}^{\text{NMSSM}} = \tilde{m}_u^2 |H_u|^2 + \tilde{m}_d^2 |H_d|^2 + \tilde{m}_S^2 |S|^2 + (\lambda A_\lambda S H_u \cdot H_d + \frac{1}{3} \kappa A_\kappa S^3 + h.c.). \quad (2)$$

In all, the Higgs sector Lagrangian contains 7 free parameters, which include

$$p_i^{\text{susy}} = \{\lambda, \kappa, \tilde{m}_u^2, \tilde{m}_d^2, \tilde{m}_S^2, A_\lambda, A_\kappa\}. \quad (3)$$

With the scalar potential expressed in term of the fields H_u , H_d and S , it is not easy to see its particle implication on the LHC results. To improve such a situation, one usually introduces following combinations of the Higgs fields[14]

$$H_1 = \cos \beta H_u + \varepsilon \sin \beta H_d^*, \quad H_2 = \sin \beta H_u - \varepsilon \cos \beta H_d^*, \quad H_3 = S, \quad (4)$$

where $\varepsilon_{12} = -\varepsilon_{21} = 1$, $\varepsilon_{11} = \varepsilon_{22} = 0$ and $\tan \beta \equiv v_u/v_d$ with v_u and v_d representing the vacuum expectation values of the fields H_u and H_d . In this representation, H_i ($i = 1, 2, 3$) are given by

$$H_1 = \begin{pmatrix} H^+ \\ \frac{S_1 + iP_1}{\sqrt{2}} \end{pmatrix}, \quad H_2 = \begin{pmatrix} G^+ \\ v + \frac{S_2 + iG^0}{\sqrt{2}} \end{pmatrix}, \quad H_3 = v_s + \frac{1}{\sqrt{2}}(S_3 + iP_2). \quad (5)$$

These expressions indicate that the field H_2 corresponds to the SM Higgs field with G^+ and G^0 denoting Goldstone bosons, and S_2 representing the SM Higgs boson (so it should make up the dominant component of the observed scalar as suggested by the LHC data), and the field H_1 represents a new $SU(2)_L$ doublet scalar field, which has no tree-level couplings to the W/Z bosons. Eq.(5) also indicates that the Higgs sector of the NMSSM includes three CP-even mass eigenstates, which are the mixtures of the fields S_1 , S_2 and S_3 , two CP-odd mass eigenstates composed by the fields P_1 and P_2 , as well as one charged Higgs H^+ .

In practical application, it is usually more convenient to use [14]

$$\lambda, \quad \kappa, \quad \tan \beta, \quad \mu, \quad M_A, \quad M_P, \quad (6)$$

as input parameters, where \tilde{m}_u^2 , \tilde{m}_d^2 and \tilde{m}_S^2 in Eq.(3) are traded for m_Z , $\tan \beta \equiv v_u/v_d$ and $\mu \equiv \lambda v_s$ by the potential minimization conditions, and A_λ and A_κ are replaced by the squared masses of the CP-odd fields P_1 and P_2 , which are given by

$$M_A^2 = \frac{2\mu}{\sin 2\beta}(A_\lambda + \kappa v_s), \quad M_P^2 = \lambda^2 v^2 \left(\frac{M_A}{2\mu/\sin 2\beta} \right)^2 + \frac{3}{2} \lambda \kappa v^2 \sin 2\beta - 3\kappa v_s A_\kappa. \quad (7)$$

Note that M_A and M_P represent the tree-level CP-odd particle masses only when the mixing between P_1 and P_2 vanishes.

With this set of input parameters, the mass matrix for CP-even Higgs bosons in the basis

(S_1, S_2, S_3) is given by[14]

$$\begin{aligned}
\mathcal{M}_{S,11}^2 &= M_A^2 + (m_Z^2 - \lambda^2 v^2) \sin^2 2\beta, \\
\mathcal{M}_{S,12}^2 &= -\frac{1}{2}(m_Z^2 - \lambda^2 v^2) \sin 4\beta, \\
\mathcal{M}_{S,13}^2 &= -(\frac{M_A^2}{2\mu/\sin 2\beta} + \kappa v_s) \lambda v \cos 2\beta, \\
\mathcal{M}_{S,22}^2 &= m_Z^2 \cos^2 2\beta + \lambda^2 v^2 \sin^2 2\beta, \\
\mathcal{M}_{S,23}^2 &= 2\lambda\mu v [1 - (\frac{M_A}{2\mu/\sin 2\beta})^2 - \frac{\kappa}{2\lambda} \sin 2\beta], \\
\mathcal{M}_{S,33}^2 &= \frac{1}{6} \lambda^2 v^2 (\frac{M_A}{\mu/\sin 2\beta})^2 + 4(\kappa v_s)^2 - \frac{1}{3} M_P^2,
\end{aligned} \tag{8}$$

and the corresponding mass eigenstates h_i ($i = 1, 2, 3$) are obtained by diagonalizing the mass matrix:

$$h_i = \sum_{j=1}^3 V_{ij} S_j,$$

where V_{ij} denotes the rotation matrix. In the following, we assume $m_{h_3} > m_{h_2} > m_{h_1}$, and call the state h_i the SM-like Higgs boson (non-SM doublet Higgs boson) if $|V_{i2}|^2 > 0.5$ ($|V_{i1}|^2 > 0.5$). Moreover, in order to present our results in a compact way we define $\bar{S}_i = V_{i3}$ and $\bar{D}_i = V_{i1}$ with $|\bar{S}_i|^2$ and $|\bar{D}_i|^2$ representing the singlet and non-SM doublet components in the physical state h_i respectively. With this notation, the couplings of h_i with vector bosons and fermions are given by

$$\begin{aligned}
C_{h_i VV}/SM &= \text{Sign}(V_{i2}) \sqrt{1 - \bar{D}_i^2 - \bar{S}_i^2}, \quad V = Z, W, \\
C_{h_i \bar{u}u}/SM &= \bar{D}_i \cot \beta + \text{Sign}(V_{i2}) \sqrt{1 - \bar{D}_i^2 - \bar{S}_i^2}, \\
C_{h_i \bar{d}d}/SM &= -\bar{D}_i \tan \beta + \text{Sign}(V_{i2}) \sqrt{1 - \bar{D}_i^2 - \bar{S}_i^2},
\end{aligned} \tag{9}$$

where the denominator SM means the corresponding Higgs coupling in the SM. We also have following sum rules

$$\begin{aligned}
\bar{D}_1^2 + \bar{D}_2^2 + \bar{D}_3^2 &= 1, \\
\bar{S}_1^2 + \bar{S}_2^2 + \bar{S}_3^2 &= 1.
\end{aligned} \tag{10}$$

The expression of $\mathcal{M}_{S,22}^2$ in Eq.(8) indicates that, without the mixings of the CP-even states, the SM-like Higgs mass at tree level is given by

$$m_{h,tree}^2 \simeq m_Z^2 \cos^2 2\beta + \lambda^2 v^2 \sin^2 2\beta,$$

where the last term on the right side is peculiar to any singlet extension of the MSSM[14], and its effect is to enhance the mass. Obviously, if the NMSSM is a natural theory, $m_{h,tree}$ should lie near 125GeV, but in practice, this is not so since the perturbativity of the theory up to GUT scale has required $\lambda \leq 0.7$ so that $m_{h,tree}^2$ usually falls far short of the desired value. For example, given $\tan \beta = 3$ and $\lambda = 0.7$, one can get $m_{h,tree} \simeq 97\text{GeV}$, which means $\Delta^2/m_{h,tree}^2 \simeq 2/3$ for the top-stop loop correction Δ^2 in order to predict the 125GeV Higgs boson in no mixing case. Confronted with such a situation, λ -SUSY, which corresponds to the NMSSM with a large λ around one, was proposed[18, 19]. This theory is based on the hypothesis that the NMSSM with a large λ is only an effective Lagrangian at the weak scale, and an appropriate structure of superfields intervenes at an ultraviolet energy scale (usually chosen at 10TeV) so that the virtues of SUSY such as the grand unification of the gauge couplings are maintained. Under this assumption, the values of λ and κ at weak scale are relaxed by[17]

$$0.17\lambda^2 + 0.26\kappa^2 \lesssim 1. \quad (11)$$

In λ -SUSY, two fine tuning quantities are defined to measure the naturalness of the theory[17]:

$$\Delta_Z = \max_i \left| \frac{\partial \log m_Z^2}{\partial \log p_i} \right|, \quad \Delta_h = \max_i \left| \frac{\partial \log m_h^2}{\partial \log p_i} \right|, \quad (12)$$

where p_i denotes SUSY parameters at the weak scale, and it includes the parameters listed in Eq.(3) and top quark Yukawa coupling Y_t with the latter used to estimate the sensitivity to stop mass. Obviously, Δ_Z (Δ_h) measures the sensitive of the weak scale (the Higgs mass) to SUSY parameters, and the larger its value becomes, the more tuning is needed to get the corresponding mass. In our calculation, we calculate Δ_Z and Δ_h by the formulae presented in [24] and [17] respectively.

Throughout this work, we consider the lightest CP-even Higgs boson as the SM-like Higgs boson. The possibility that the next-to-lightest CP-even Higgs boson corresponds to the SM-like Higgs boson is theoretically less appealing since $m_{h,tree}$ in λ -SUSY usually exceeds 125GeV, and the mixing of S_2 and S_3 can further push up the mass so that the theory has more tuning to get the Higgs boson mass. Our numerical scan checked this point.

B. Strategy in Scanning the Parameter Space of λ -SUSY

In this work, we first perform a comprehensive scan over the parameter space of λ -SUSY by considering various experimental constraints. Then for the surviving samples we investigate the features of its Higgs sector. In order to simplify our analysis, we make following assumptions about some unimportant SUSY parameters:

- First, we fix all soft breaking parameters for the first two generation squarks at 2TeV. For the third generation squarks, considering that they can affect significantly the mass of the SM-like Higgs boson, we set free all soft parameters in this sector except that we assume $m_{U_3} = m_{D_3}$ for right-handed soft breaking masses and $A_t = A_b$ for soft breaking trilinear coefficients.
- Second, since we require λ -SUSY to explain the discrepancy of the measured value of the muon anomalous magnetic moment from its SM prediction, we assume all soft breaking parameters in the slepton sector to have a common value $m_{\tilde{l}}$ and treat $m_{\tilde{l}}$ as a free parameter.
- Third, we assume the grand unification relation $3M_1/(5\alpha_1) = M_2/\alpha_2$ for electroweak gaugino masses, and set gluino mass at 2TeV.

With above assumptions, we use the package NMSSMTools-4.0.0 [25] to scan following parameter space of λ -SUSY:

$$\begin{aligned}
0.7 < \lambda \leq 2, \quad 0 < \kappa \leq 2, \quad 100 \text{ GeV} \leq M_A, M_P, \mu \leq 3 \text{ TeV}, \\
100 \text{ GeV} \leq M_{Q_3}, M_{U_3} \leq 2 \text{ TeV}, \quad |A_t| \leq 5 \text{ TeV}, \\
1 \leq \tan \beta \leq 15, \quad 100 \text{ GeV} \leq m_{\tilde{l}}, M_2 \leq 1 \text{ TeV},
\end{aligned} \tag{13}$$

where all the parameters are defined at the scale of 1TeV. During the scan, we keep samples that satisfy following constraints:

- (1) The SM-like Higgs boson lies around 125GeV: $124\text{GeV} \leq m_h \leq 126\text{GeV}$, $m_{\tilde{l}_i} \geq 200\text{GeV}$ as suggested by the LHC search for stops[26, 27], and also the bound on λ, κ from Eq.(11).
- (2) All the constraints implemented in the package NMSSMTools-4.0.0, which are from the vacuum stability (including the absence of charge and color breaking), the LEP results

in sparticle search including the lower bounds on various sparticle masses and the upper bounds on the chargino/neutralino pair production rates, the Z -boson invisible decay, the B -physics observables such as the branching ratios for $B \rightarrow X_s \gamma$ and $B_s \rightarrow \mu^+ \mu^-$, and the mass differences ΔM_d and ΔM_s , the discrepancy of the muon anomalous magnetic moment, the dark matter relic density and the LUX limits on the scattering rate of dark matter with nucleon. In getting the constraint from a certain observable which has an experimental central value, we use its latest measured result and require the NMSSM to explain the result at 2σ level.

- (2) Constraints from the search for Higgs bosons at the LEP, the Tevatron and the LHC. We implement these constraints with the package HiggsBounds-4.0.0 [28].
- (3) Indirect constraints from the electroweak precision data such as ρ_ℓ , $\sin^2 \theta_{eff}^\ell$, M_W and R_b . We require all these quantities in the NMSSM within the 2σ range of their experimental values. We compute these observables with the formula presented in [20]. Note these constraints are important in limiting $\tan \beta$ in λ -SUSY [19, 20].

For each surviving sample, we further perform a fit by using the Higgs data updated in this summer. These data include the measured signal strengthes for $\gamma\gamma$, ZZ^* , WW^* , $b\bar{b}$ and $\tau\bar{\tau}$ channels, and their explicit values are shown in Fig.2 of [5], Fig.20 of [6] and Fig.20 of [7] for the ATLAS results, in Fig.5 of [8] for the CMS results and in Fig.15 of [29] for the CDF+D0 results. We totally use 26 sets of experimental data with 24 of them corresponding to the measured signal strengthes and the other 2 being the combined masses of the Higgs boson reported by the ATLAS and the CMS collaborations respectively. In calculating corresponding χ^2 , we use the method first introduced in [30], and consider the correlations among the data like done in [31]. For the surviving samples, we obtain $\chi_{min,2014}^2/d.o.f = 12.1/15$, where $\chi_{min,2014}^2$ represents the minimal value of the χ^2 with the Higgs data in 2014, and the total number of the degree of freedom (d.o.f.) is counted in a naive way as $\nu = n_{obs} - n_{para}$ [12] with $n_{obs} = 26$ denoting the set number of the experimental data and $n_{para} = 11$ being the number of the model free parameters listed in Eq.(13). In the following, we concentrate on the samples satisfying $\chi^2 \leq 25$. These samples are interpreted in statistics as the points that keep consistency with the Higgs data at 95% C.L..

Compared with the similar fit done in 2013 (see for example that in [32]), we find $\chi_{min,2013} \simeq 17$ for the same set of the surviving samples, which is significantly larger than

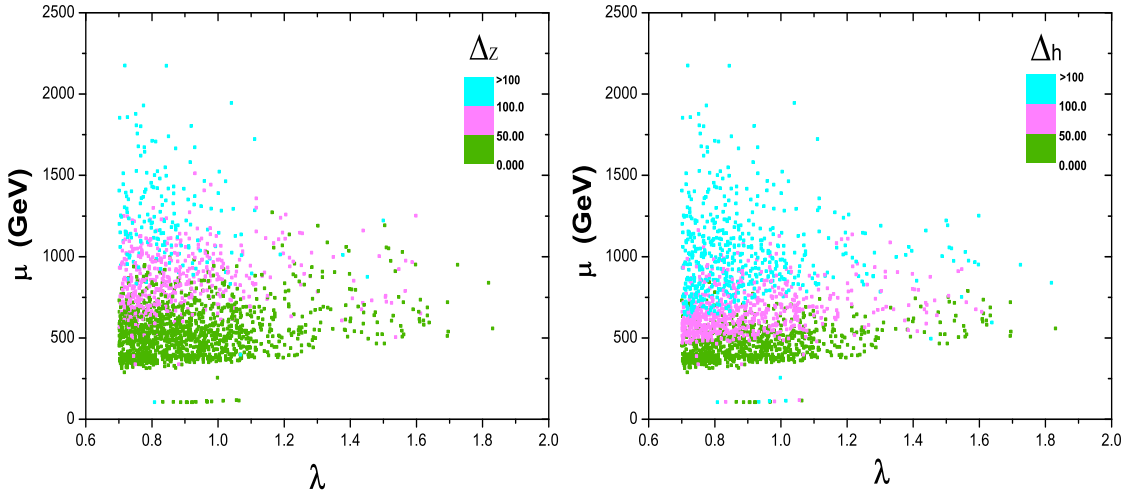


FIG. 1: Samples surviving the constraints 1-3 and meanwhile satisfying $\chi^2 \leq 25$, projected on the plane of μ versus λ . For these samples, their predictions on the fine tuning parameters Δ_Z and Δ_h are marked with different colors.

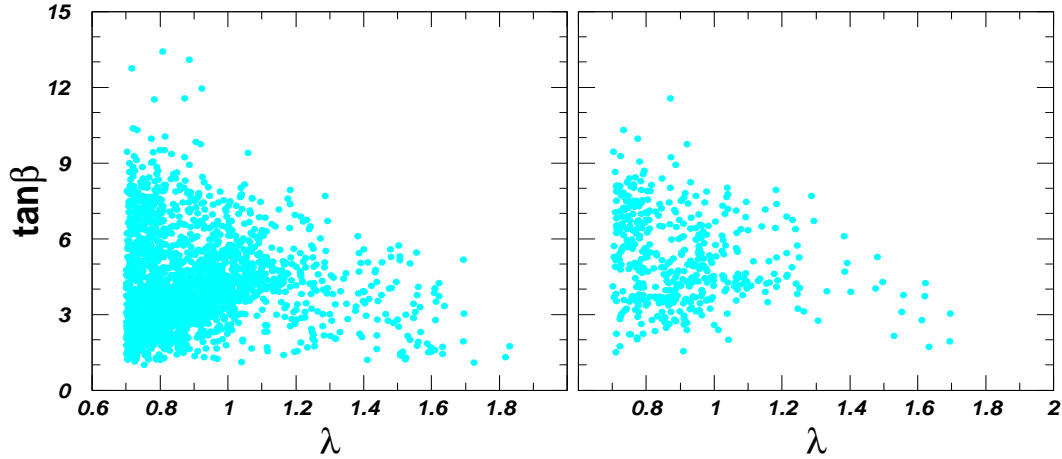


FIG. 2: Surviving samples projected on $\tan \beta - \lambda$ plane. Samples in the left panel are same as that of Fig.1, while samples in the right panel are further required to satisfy $\max\{\Delta_Z, \Delta_h\} \leq 50$.

$\chi_{min,2014}$. This reflects the more consistency of the two collaboration results in describing the properties of the discovered boson.

At this stage, we emphasize that since the main advantage of λ -SUSY over the MSSM is its naturalness in predicting m_Z and m_h , Δ_Z and Δ_h should be used as a criteria in estimating the goodness of the parameter points, that is, samples with very large Δ_Z and Δ_h should be viewed as theoretically disfavored even though they may agree well with various measurements. Numerically speaking, considering that Δ_Z in the MSSM are usually larger

than 50[11] (note the definition of Δ_Z in [11] differs from that in this work by a factor 2), we take $\max\{\Delta_Z, \Delta_h\} \leq 50$ as a standard for naturalness. To exhibit the characters of Δ_Z and Δ_h in λ -SUSY, in Fig.1 we project the surviving samples on the plane of μ versus λ with their corresponding values of Δ_Z and Δ_h marked with different colors. This figure indicates that the samples with relatively low Δ_Z and Δ_h are usually associated with a low μ , or numerically speaking, requiring $\max\{\Delta_Z, \Delta_h\} \leq 50$ results in $\mu \lesssim 780\text{GeV}$. This can be intuitively understood by the fact that $\mu = \lambda v_s$ with the natural size of v_s lying at the weak scale. Furthermore, we checked that, for most of the surviving samples, Δ_Z and Δ_h are more sensitive to λ than to the other SUSY parameters.

Since λ and $\tan\beta$ are two most important parameters in λ -SUSY, we pay particular attention to their correlation. In Fig.2 we show all the surviving samples on the $\tan\beta - \lambda$ plane without and with the requirement $\max\{\Delta_Z, \Delta_h\} \leq 50$ (see left panel and right panel respectively). This figure indicates that, with the increase of λ , $\tan\beta$ tends to decrease and for $\lambda > 1$, $\tan\beta \leq 15$. The main reason for such a behavior is, as we mentioned before, due to the constraints from the electroweak precision data. This figure also indicates that, after requiring $\max\{\Delta_Z, \Delta_h\} \leq 50$, a large portion of samples with relatively low values of $\tan\beta$ are excluded. The reason is that $m_{h,\text{tree}}^2$ in λ -SUSY is usually larger than 125GeV and a high value of $\tan\beta$ tends to narrow the mass gap.

Based on above arguments and meanwhile in order to show the preference of the Higgs data and the fine tuning argument on the parameter space, we classify the surviving samples into three types as follows:

- Type-I samples: those with $\chi^2 \leq 25$ and meanwhile $\max\{\Delta_Z, \Delta_h\} \leq 50$. This type of sample is considered as the physical sample in our discussion.
- Type-II samples: those with $\chi^2 \leq 25$ but $\max\{\Delta_Z, \Delta_h\} > 50$. This type of sample can not be excluded by experiments, but is not favored by the fine tuning argument.
- Type-III samples: those with $\chi^2 > 25$. Obviously, this type of sample is of less interest than the previous two types.

For completeness, we present in Table I the allowed ranges for these samples. As shown in Fig.1 and Fig.2 and also in this Table, with the increase of λ , the parameter space of λ -SUSY are crushed into a narrow region until λ reaches its maximum, which is about 1.8.

TABLE I: Allowed ranges for different parameters. All types of samples survive the constraints 1-3, and they differ only by their predictions on χ^2 and $\max\{\Delta_Z, \Delta_h\}$ (see their definitions at the end of Subsection B).

Parameters	Type-I Samples	Type-(I+II) Samples	Type-(I+II+III) Samples
λ	$0.7 \sim 1.8$	$0.7 \sim 1.8$	$0.7 \sim 2$
κ	$0.2 \sim 1.9$	$0.1 \sim 1.9$	$0.1 \sim 1.9$
$\tan \beta$	$1.2 \sim 13$	$1 \sim 13.4$	$1 \sim 15$
$\mu(\text{GeV})$	$105 \sim 780$	$105 \sim 2180$	$100 \sim 2200$
$M_A(\text{GeV})$	$365 \sim 3000$	$350 \sim 3000$	$340 \sim 3000$
$M_P(\text{GeV})$	$65 \sim 3000$	$65 \sim 3000$	$20 \sim 3000$
$M_1(\text{GeV})$	$50 \sim 470$	$50 \sim 500$	$50 \sim 500$
$M_{Q_3}(\text{GeV})$	$200 \sim 2000$	$200 \sim 2000$	$200 \sim 2000$
$M_{U_3}(\text{GeV})$	$200 \sim 2000$	$200 \sim 2000$	$200 \sim 2000$
$A_t(\text{GeV})$	$-4350 \sim 4300$	$-5000 \sim 4800$	$-5000 \sim 5000$
$M_{\tilde{l}}(\text{GeV})$	$100 \sim 520$	$100 \sim 530$	$100 \sim 530$
$A_\lambda(\text{GeV})$	$-1100 \sim 2900$	$-2800 \sim 2900$	$-2800 \sim 3000$
$A_\kappa(\text{GeV})$	$-2600 \sim 130$	$-2600 \sim 205$	$-2600 \sim 560$

III. PROPERTIES OF h_1 AND h_2

In this section, we explore the Higgs sector of λ -SUSY to exhibit the properties of the lightest and the next-to-lightest CP-even Higgs bosons. We pay particular attention to the features of the bosons that differentiate λ -SUSY from the MSSM or from the NMSSM with a low λ .

A. Properties of the Lightest CP-even Higgs Boson

As we mentioned before, throughout this work we treat the lightest CP-even Higgs boson as the SM-like Higgs boson, so some properties of h , such as its coupling to vector bosons, have been limited to closely mimic those of the SM Higgs boson. However, as we will show below, the triple self coupling of the boson or more general the Higgs potential may still differ greatly from that of the SM.

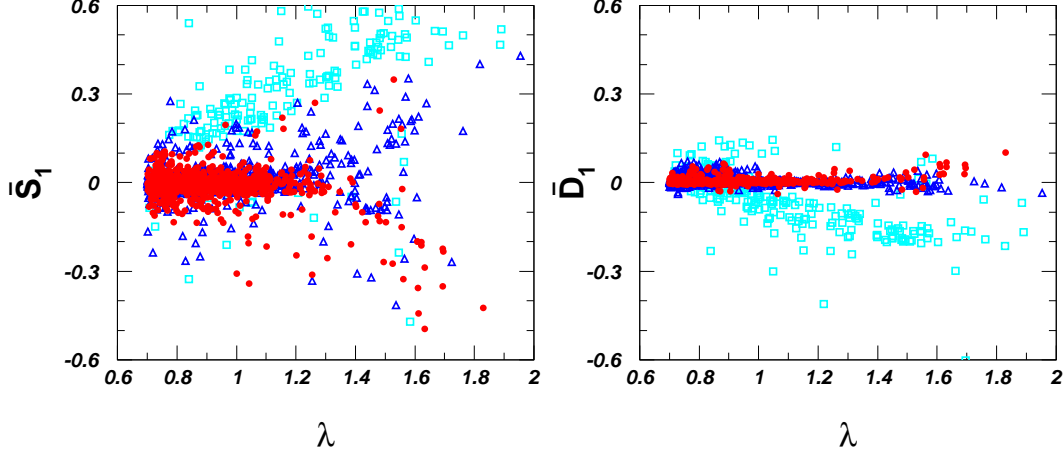


FIG. 3: Singlet component coefficient \bar{S}_1 and non-SM doublet component coefficient \bar{D}_1 of the SM-like Higgs boson as a function of λ . Here red bullet, blue triangle and sky-blue square denote Type-I sample, Type-II sample and Type-III sample respectively.

In Fig.3, we show the singlet component coefficient \bar{S}_1 and non-SM doublet component coefficient \bar{D}_1 of h for Type-I samples (red bullet), Type-II samples (blue triangle) and Type-III samples (sky-blue square) on the left panel and right panel respectively. This figure indicates that, without considering the Higgs data $|\bar{S}_1|$ may exceed 0.6, and after considering the data, it is up bounded by about 0.5 at 95% C.L.. In contrast, $|\bar{D}_1|$ reaches at most about 0.3 and 0.1 before and after considering the data respectively, and given $\bar{S}_1 \neq 0$, it is always much smaller than $|\bar{S}_1|$ after considering the data. The reason for the difference between \bar{S}_1 and \bar{D}_1 is that the constraints we considered have put non-trivial requirements on the elements \mathcal{M}_{11}^2 and \mathcal{M}_{12}^2 of the CP-even Higgs mass matrix, e.g. $\mathcal{M}_{11}^2 \gtrsim 200\text{GeV}^2$ and $|\mathcal{M}_{12}^2/\mathcal{M}_{11}^2| \ll 1$, so $|\bar{D}_1|$ is forbidden to be moderately large. In comparison, \mathcal{M}_{33}^2 is less constrained due to the singlet nature of the field S_3 , and given $\mathcal{M}_{33}^2 \simeq \mathcal{M}_{22}^2$, $|\bar{S}_1|$ may be as large as 0.7. Furthermore, from the coupling expressions of h in Eq.(9) one can learn that, due to the non-vanishing of \bar{S}_1 and \bar{D}_1 , the hZZ coupling is always suppressed in comparison with its SM value, while for the fermion Yukawa couplings $Y_{h\bar{f}f}$, depending the sign of \bar{D}_1 , it may be either enhanced or suppressed. Explicitly speaking, given $\bar{S}_1 = 0$ and $|\bar{D}_1| < 0.1$, one can learn that $C_{h\bar{u}u}$ is enhanced while $C_{h\bar{d}d}$ is suppressed if \bar{D}_1 is positive, and the situation reverses for the two couplings if \bar{D}_1 changes sign. In any case, the larger $|\bar{S}_1|$ becomes, the smaller the couplings are. Fig.3 also indicates that, with the increase of λ , $|\bar{S}_1|$ and $|\bar{D}_1|$ tend to increase too, and so are the deviations of the normalized couplings from unity. The reason is, given a sufficient large λ , $m_{h,tree}$ will be much larger than 125GeV,

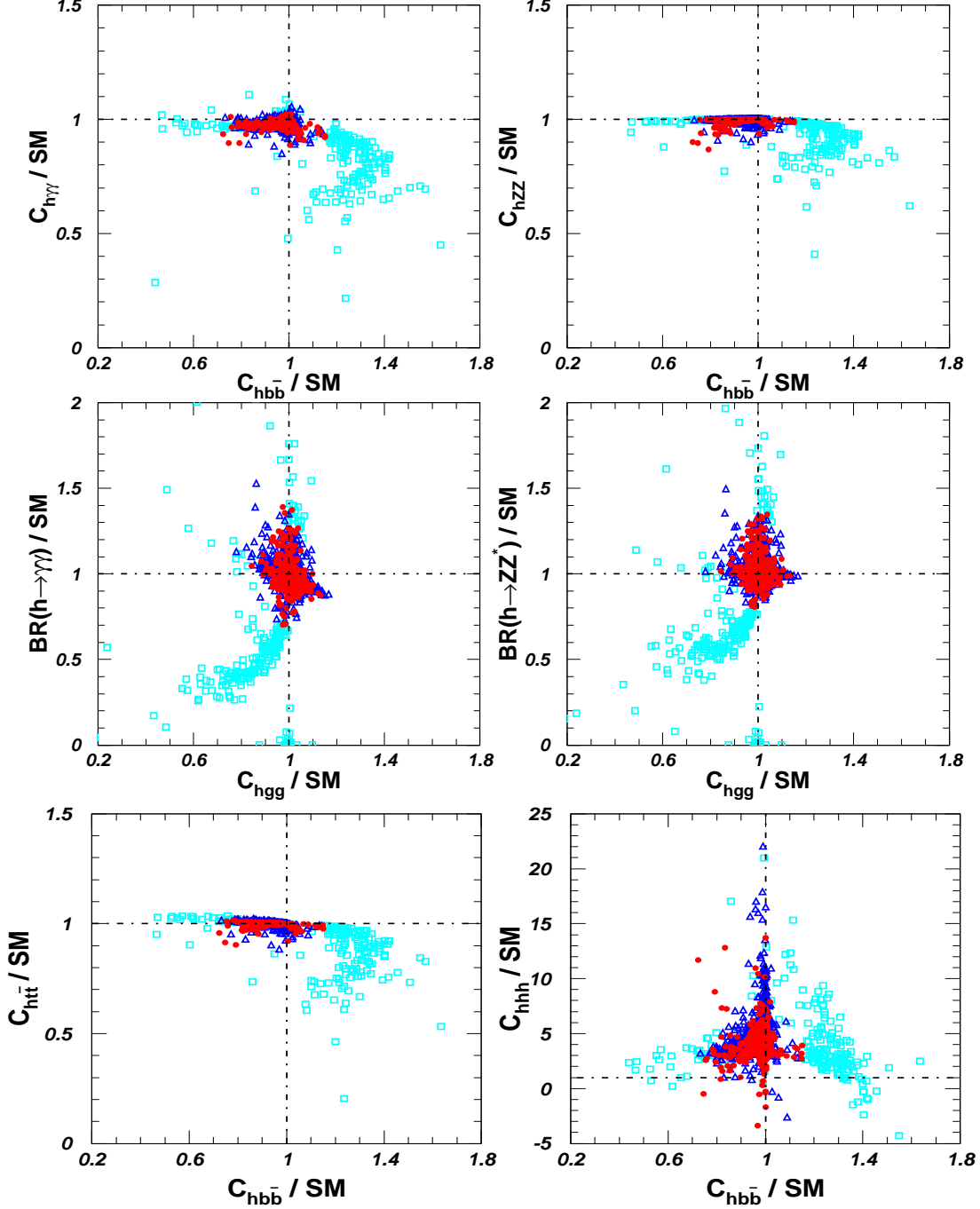


FIG. 4: Coupling information of the SM-like Higgs boson for Type-I sample (red bullet), Type-II sample (blue triangle) and Type-III sample (sky-blue square).

and sizable mixings must intervene to pull down the mass.

We also compare our results in Fig.3 with those in [17], where a similar fit was performed by using the Higgs data in 2013 in the framework of λ -SUSY. We find that now the allowed ranges of $|\bar{S}_1|$ and $|\bar{D}_1|$ shrink significantly. This reflects the more tightness of the new data

in limiting the Higgs properties.

Now let's turn to the couplings of h . In Fig.4, we exhibit such information for same samples as those in Fig.3. This figure indicates that, after imposing the constraints from the Higgs data, the normalized couplings $C_{h\gamma\gamma}/SM$, C_{hZZ}/SM and $C_{h\bar{t}t}/SM$ are limited within 10% deviation from unity, and the couplings C_{hgg}/SM and $C_{h\bar{b}b}/SM$ are allowed to vary in relatively wider ranges, at most 20% and 30% deviating from unity respectively. Moreover, due to the change of the width of h , which is mainly determined by $C_{h\bar{b}b}$, the normalized branching ratios $Br(h \rightarrow \gamma\gamma)/SM$ and $Br(h \rightarrow ZZ^*)/SM$ may vary from 0.8 to 1.5. Compared with the similar fit results in 2012[11], we find in the new fit that the optimal values of the couplings are shifted significantly.

Maybe the most impressive feature of h in λ -SUSY is that the strength of its triple self coupling C_{hhh}/SM may get enhanced by a factor over 10. This is shown on the right panel of the third row in Fig.4, which exhibits that C_{hhh}/SM may reach 14 and 22 for the Type-I samples and Type-II samples respectively. Here We remind that that such a great enhancement can not occur in the MSSM where the quartic terms of the Higgs potential are determined by the weak coupling[33]. We also remind that the enhancement seems to be limited by the naturalness argument. To see this, we list two benchmark points with large C_{hhh} in Table II (see points P1 and P2). One can easily learn that each point corresponds to a low Higgs χ^2 , but a large Δ_Z and Δ_h , indicating that naturalness disfavor a too large C_{hhh} in λ -SUSY.

B. Properties of the Next-to-Lightest CP-even Higgs Boson

Considering that h_3 in λ -SUSY is usually at TeV scale and thus it decouples from the electroweak physics, we here only study the property of the Next-to-Lightest CP-even Higgs boson h_2 . As we will show below, such a study is helpful to understand the Higgs pair production process.

In Fig.5, we show the non-SM doublet component \bar{D}_2^2 as a function of m_{h_2} for Type-I, Type-II and Type-III samples. This figure reveals following information:

- For $m_{h_2} \leq 500\text{GeV}$, \bar{D}_2^2 is either around 1 or around 0 for Type-I and Type-II samples. In this case, the mixing between the fields S_1 and S_3 is small in forming h_2 , which can be obtained if $|\mathcal{M}_{13}^2| \ll |\mathcal{M}_{11}^2 - \mathcal{M}_{33}^2|$. Note such a situation is not altered until

TABLE II: Benchmark points for different cases considered in this work. Note all the input parameters are defined at 1TeV, and in calculating the spectrum of the Higgs bosons, important radiative corrections have been taken into account.

No. of Point	Point 1 (P1)	Point 2 (P2)	Point 3 (P3)	Point 4 (P4)
λ	0.86	0.94	0.75	0.71
κ	1.27	1.19	1.64	1.64
$\tan \beta$	1.59	1.82	1.45	1.35
$\mu(\text{GeV})$	697.6	1100.7	614.0	599.8
$M_A(\text{GeV})$	2127.9	2237.9	388.1	372.6
$M_P(\text{GeV})$	1449.4	283.8	2282.4	2135.2
$M_1(\text{GeV})$	169.9	200.7	83.2	70.5
$M_{Q_3}(\text{GeV})$	1646.3	675.5	409.2	1587.8
$M_{U_3}(\text{GeV})$	511.0	1435.6	697.6	894.7
$M_{\tilde{l}}(\text{GeV})$	186.5	218.5	128.4	112.4
$A_t(\text{GeV})$	-25.1	1539.6	881.1	-1639.8
$A_\lambda(\text{GeV})$	766.0	-310.5	-1248.9	-1302.0
$A_\kappa(\text{GeV})$	-674.5	-12.5	-1602.3	-1032.6
$m_h(\text{GeV})$	125.0	125.4	125.2	124.4
$m_{H_2}(\text{GeV})$	1697.3	2144.6	232.4	245.0
$m_{A_1}(\text{GeV})$	1440.5	174.0	150.5	102.3
$m_{H^\pm}(\text{GeV})$	2088.2	2153.7	228.1	238.6
\bar{D}_1	-8×10^{-5}	2×10^{-3}	0.01	0.04
\bar{S}_1	0.02	-0.02	6×10^{-3}	-3×10^{-3}
\bar{D}_2	-0.22	-0.98	-0.99	-0.99
\bar{D}_{A_1}	0.08	0.10	0.99	0.99
χ^2	12.7	12.5	12.4	17.4
Δ_Z	35.4	139.6	46.9	45.1
Δ_h	38.4	233.2	89.5	89.1
C_{hhh}/SM	13.7	22.1	5.1	4.2
$\sigma(gg \rightarrow hh)/SM$	34.3	96.1	1.3	0.6

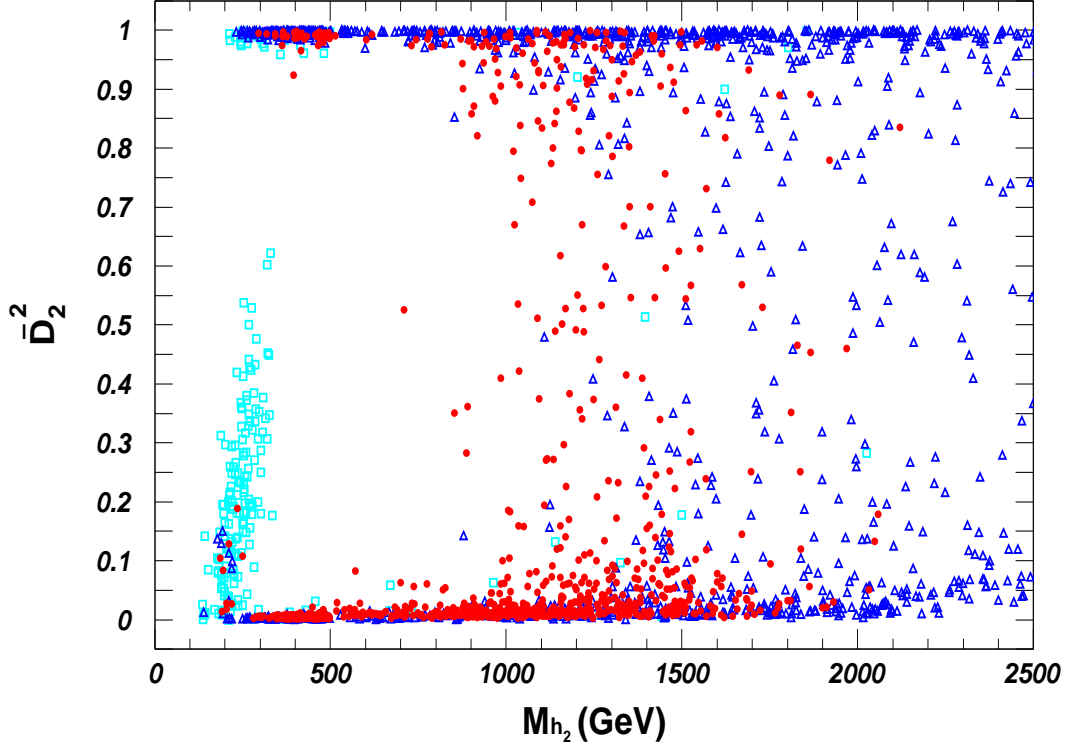


FIG. 5: Doublet component of h_2 as a function of m_{h_2} for the same samples as Fig.3. Again, Type-I, Type-II and Type-III samples are marked with red bullet, blue triangle and sky-blue square, respectively.

$$m_{h_2} \gtrsim 800 \text{ GeV}.$$

- In case of $\bar{D}_2^2 \simeq 1$, h_2 is obviously non-SM doublet dominated, while in case of $\bar{D}_2^2 \simeq 0$, h_2 should be singlet dominated since $\bar{D}_3^2 = 1 - \bar{D}_1^2 - \bar{D}_2^2 \simeq 1$, which implies that h_3 is non-SM doublet dominated.
- The doublet dominated h_2 can be as light as 200 GeV, which is quite different from the situation of the MSSM where the non-SM Higgs boson H must be heavier than about 300 GeV after considering various constraints[34]. As a comparison, the singlet dominated h_2 is more loosely limited so that it can be lighter than 150 GeV.
- Note for $m_{h_2} \lesssim 300 \text{ GeV}$, there exist some type-III samples with $\bar{D}_2^2 > 0.2$. Since $\bar{D}_3^2 = 1 - \bar{D}_1^2 - \bar{D}_2^2 < 0.8$, these samples predict a h_3 with sizable singlet and/or SM doublet components. This mixing pattern can be achieved only for a not too heavy h_3 . In fact, we examined the properties of these sample, and found $m_{h_3} \lesssim 650 \text{ GeV}$ and $\mu \lesssim 200 \text{ GeV}$. Since all CP-even Higgs bosons in this case are relatively light, it

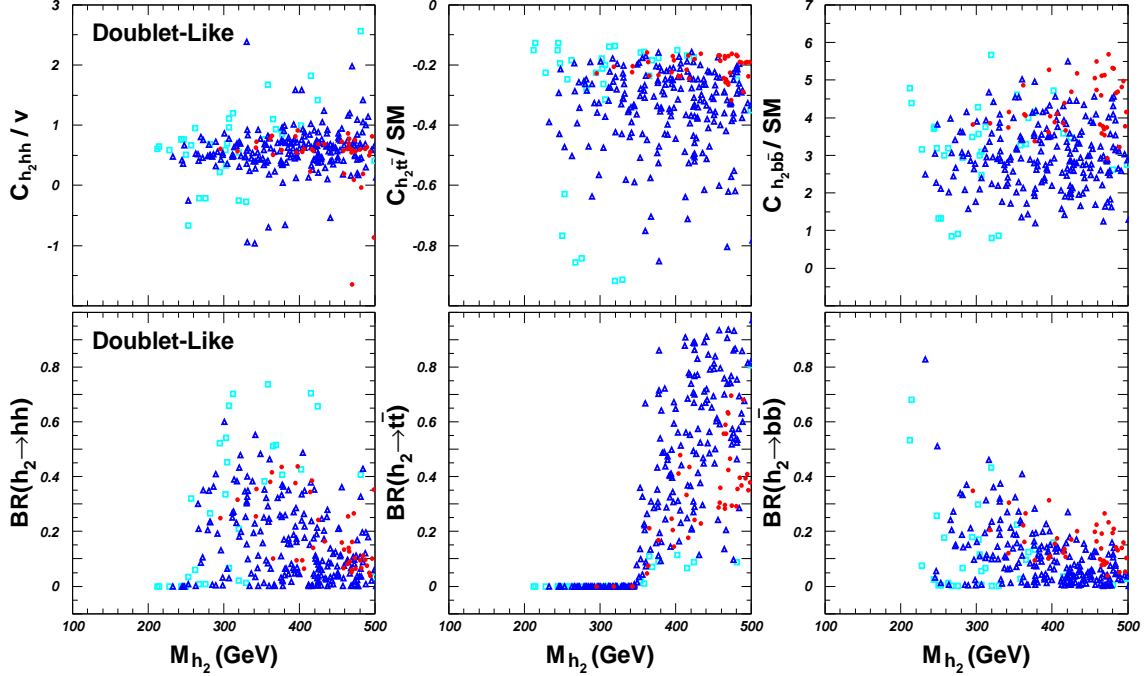


FIG. 6: Couplings and Branching ratios of h_2 as a function of h_2 . Note that only the samples with doublet dominated h_2 in Fig.6 are considered.

is apt to be tightly limited by the Higgs data.

- Naturalness should play a role in limiting the properties of h_2 [35]. Explicitly speaking, Fig.5 shows that there are few Type-I samples with $m_{h_2} > 2000\text{GeV}$, which may be interpreted as that naturalness prefers a relatively light h_2 . Another example is the fraction of Type-I samples in the total number of Type-I plus Type-II samples for the doublet dominated h_2 is significantly lower than that for the singlet dominated h_2 , which means that naturalness tends to put a tighter constraint on the doublet dominated h_2 . All these features can be intuitively understood by the fact that, since $v_u, v_d \sim 100\text{GeV}$, a too heavy non-SM doublet dominated h_2 will make the theory fine tuned to get the correct electroweak symmetry breaking.

In the following, we try to illustrate the properties of h_2 for Type-I and Type-II samples with $m_{h_2} \leq 500\text{GeV}$. These samples are characterized by either $\bar{D}_2^2 \simeq 1$ or $\bar{D}_2^2 \simeq 0$, which is very helpful to simplify our analysis.

We first concentrate on a doublet dominated h_2 . Since $\bar{D}_2^2 \simeq 1$, the couplings of the h_2 can be approximated by:

$$C_{h_2 VV}/SM \simeq 0, \quad C_{h_2 \bar{u}u}/SM \simeq \text{Sign}(\bar{D}_2) \cot \beta, \quad C_{h_2 \bar{d}d}/SM \simeq -\text{Sign}(\bar{D}_2) \tan \beta. \quad (14)$$

In Fig.6, we only consider the doublet dominated h_2 in Fig.5 and show their normalized couplings such as $C_{h_2\bar{t}t}/SM$, $C_{h_2\bar{b}b}/SM$ and C_{h_2hh}/v as functions of m_{h_2} . We also plot the branching ratios of $h_2 \rightarrow \bar{t}t$, $h_2 \rightarrow \bar{b}b$ and $h_2 \rightarrow hh$ in a similar way.

From Fig.6, we can learn following features about Type-I and Type-II samples:

- In most cases, Eq.(14) is a good approximation for the three h_2 couplings, especially for the coupling $C_{h_2\bar{b}b}/SM$.
- In general, with the increase of m_{h_2} , the couplings $C_{h_2\bar{t}t}/SM$ and $C_{h_2\bar{b}b}/SM$ can vary within a wider ranges. This is because the constraints we considered get relaxed as h_2 becomes heavier so that the couplings become more flexible to satisfy the constraints. This character also applies to the singlet dominated h_2 .
- $|C_{h_2\bar{t}t}/SM|$ is not too small: $|C_{h_2\bar{t}t}/SM| \gtrsim 0.2$, and in optimal case, it is just slightly below 1. On the other hand, $|C_{h_2\bar{b}b}/SM|$ is usually larger than one with its maximum value reaching 6. In this case, the h_2gg coupling is given by

$$\begin{aligned} \left| \frac{C_{h_2gg}}{C_{hgg}^{SM}} \right| &\simeq \frac{\cot \beta A_{\frac{1}{2}}\left(\frac{m_{h_2}^2}{4m_t^2}\right) - \tan \beta A_{\frac{1}{2}}\left(\frac{m_{h_2}^2}{4m_t^2}\right)}{A_{\frac{1}{2}}\left(\frac{m_{h_2}^2}{4m_t^2}\right)} \\ &\simeq \begin{cases} \{1.5 \cot \beta - (-0.03 + 0.03i) \tan \beta\}/1.4 & \text{for } m_{h_2} = 250\text{GeV}, \\ \{(2.0 + 0.01i) \cot \beta - (-0.02 + 0.02i) \tan \beta\}/1.4 & \text{for } m_{h_2} = 350\text{GeV}, \\ \{(2.1 + 1.1i) \cot \beta - (-0.01 + 0.01i) \tan \beta\}/1.4 & \text{for } m_{h_2} = 450\text{GeV}, \\ \{(1.5 + 1.6i) \cot \beta - (-0.01 + 0.01i) \tan \beta\}/1.4 & \text{for } m_{h_2} = 550\text{GeV}, \end{cases} \end{aligned}$$

where the loop function $A_{\frac{1}{2}}$ is defined in [33] and we have neglected the minor important squark contribution. This expression indicates that, due to the opposite sign of the two couplings, the real parts of the top and bottom contributions to the ggh_2 interaction interfere constructively while the imaginary parts interfere destructively, and the h_2gg coupling strength is maximized at low $\tan \beta$.

- The potentially important decay modes of h_2 include $h_2 \rightarrow \bar{t}t, \bar{b}b, A_1A_1, \tilde{\chi}_i\tilde{\chi}_j$, where A_1 denotes the lighter CP-odd Higgs boson and $\tilde{\chi}_i$ represents a supersymmetric particle such as a neutralino. For $m_{h_2} \gtrsim 400\text{GeV}$, $h_2 \rightarrow \bar{t}t$ is usually the main decay mode, for $260\text{GeV} \lesssim m_{h_2} \lesssim 400\text{GeV}$, $h_2 \rightarrow hh$ may be dominant over the other channels and for $m_{h_2} \lesssim 250\text{GeV}$, any of the decays $h_2 \rightarrow \bar{b}b, A_1A_1, \tilde{\chi}_i\tilde{\chi}_j$ may become the most important.

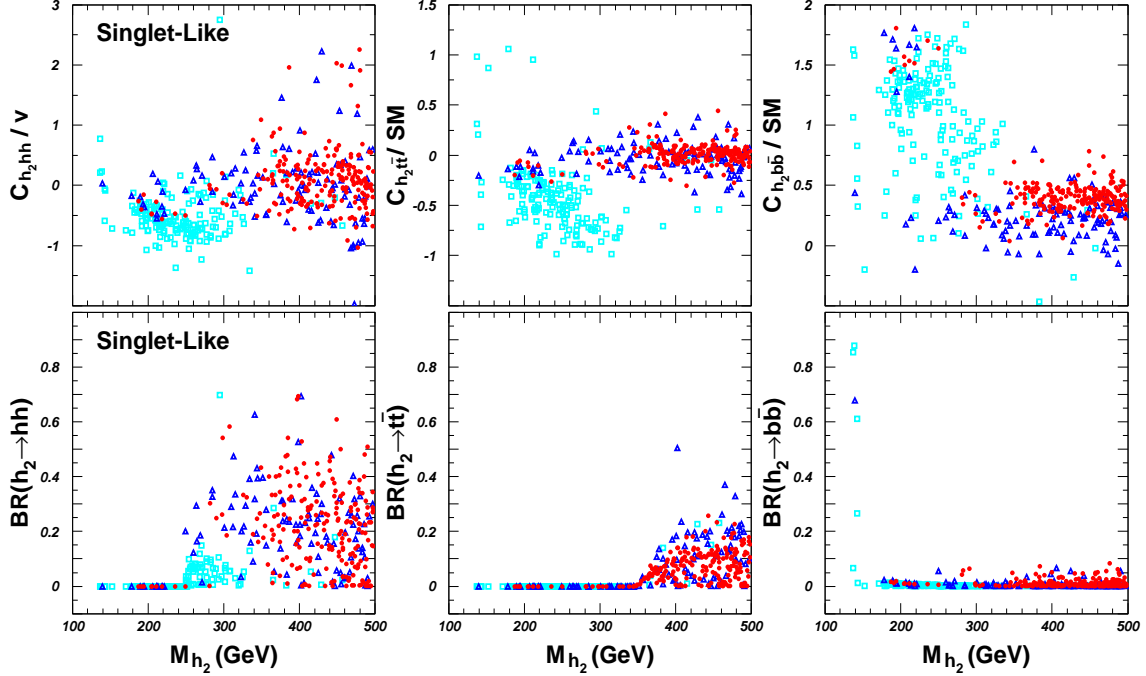


FIG. 7: Same as Fig.6, but for a singlet dominated h_2 .

- Considering that the case of $m_{h_2} \lesssim 250\text{GeV}$ was scarcely studied before, we pay particular attention to its features. We find the Higgs sector in this case usually exhibits an inverted mass hierarchy, i.e. the spectrum is characterized by $m_{h_2} \simeq m_{H^\pm} > m_{A_1}$ instead of the usual order $m_{A_1} > m_{H^\pm}$. The underlying reason for such an anomaly is owe to the hierarchy structure of the CP-odd Higgs mass matrix in the basis (P_1, P_2) : $|\mathcal{M}_{P,11}^2| \ll |\mathcal{M}_{P,12}^2| \ll |\mathcal{M}_{P,21}^2|$. For such a mass matrix, the physical scalar A_1 can be tuned to be very light by choosing an appropriate value of $\mathcal{M}_{P,12}^2$. In Table II, we list two such points (denoted by P3 and P4 respectively) with P3 further satisfying $m_{h_2} > 2m_{A_1}$.

Next we consider the singlet dominated h_2 . In this case, since $\bar{D}_2^2 \simeq 0$, we have

$$1 - \bar{S}_2^2 - \bar{D}_2^2 \simeq 1 - \bar{S}_2^2 \simeq \bar{S}_1^2 + \bar{S}_3^2, \quad (15)$$

where the sum rule $\bar{S}_2^2 = 1 - \bar{S}_1^2 - \bar{S}_3^2$ is used. On the other hand, because

$$\bar{S}_3^2 + \bar{D}_3^2 = \bar{S}_3^2 + 1 - \bar{D}_2^2 - \bar{D}_1^2 \simeq \bar{S}_3^2 + 1 - \bar{D}_1^2 \leq 1,$$

we get

$$\bar{S}_3^2 \lesssim \bar{D}_1^2. \quad (16)$$

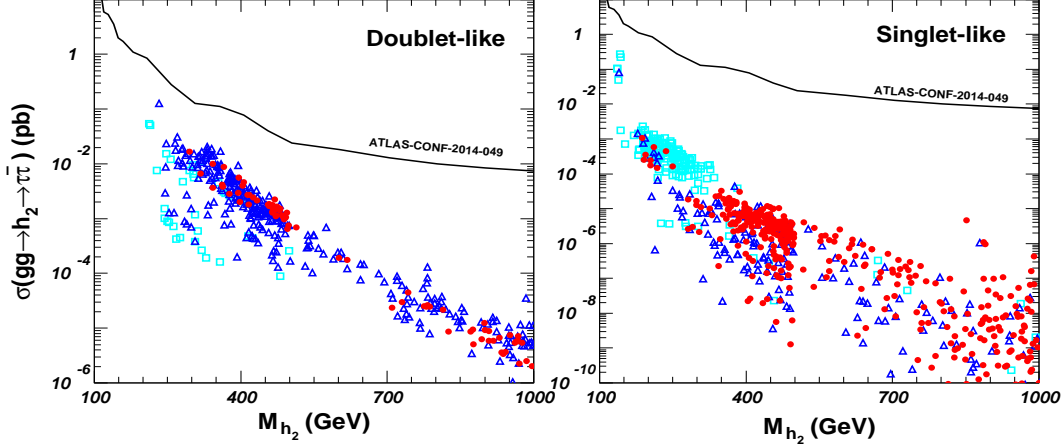


FIG. 8: Same as Fig.6 (left panel) and Fig.7 (right panel), but showing the $\bar{\tau}\tau$ signal rates induced by the process $gg \rightarrow h_2 \rightarrow \bar{\tau}\tau$ at 8-TeV LHC. As a comparison, the bounds from the direct search for $\bar{\tau}\tau$ signal by ATLAS collaboration are also shown.

Taking Eq.(15) and Eq.(16) in mind, and noticing the fact that $\bar{D}_1^2 \ll \bar{S}_1^2$ for sizable \bar{S}_1 (see discussion about Fig.3), we finally conclude that

$$1 - \bar{S}_2^2 - \bar{D}_2^2 \simeq \bar{S}_1^2. \quad (17)$$

With this approximation, we can write down the couplings of the singlet dominated h_2 as:

$$\begin{aligned} C_{h_2 VV}/SM &\simeq |\bar{S}_1|, & C_{h_2 \bar{u}u}/SM &\simeq \text{Sign}(V_{22})|\bar{S}_1|, \\ C_{h_2 \bar{d}d}/SM &\simeq -\bar{D}_2 \tan \beta + \text{Sign}(V_{22})|\bar{S}_1|. \end{aligned} \quad (18)$$

In Fig.7, we show the couplings $C_{h_2 \bar{t}t}/SM$, $C_{h_2 \bar{b}b}/SM$ and $C_{h_2 hh}/v$, and also the branching ratios of $h_2 \rightarrow \bar{t}t$, $h_2 \rightarrow \bar{b}b$ and $h_2 \rightarrow hh$ in a way similar to Fig.6. This figure indicates that, as suggested by above approximations, both the $h_2 \bar{t}t$ and $h_2 \bar{b}b$ couplings for a singlet-like h_2 are usually small, but the coupling $h_2 hh$ may still be large with $C_{h_2 hh}/v$ reaching about 2.5 in optimal case. As a result of such couplings and meanwhile the relatively strong interaction of the h_2 with sparticles[50], $h_2 \rightarrow \bar{t}t$ is no longer the dominant decay channel of h_2 even for $m_{h_2} \gtrsim 400\text{GeV}$, instead any of $h_2 \rightarrow hh$, $A_1 A_1$, $\tilde{\chi}_i \tilde{\chi}_j$ may become dominant once the kinematics is accessible. We checked that, for $m_{h_2} < 250\text{GeV}$, $h_2 \rightarrow \tilde{\chi}_i \tilde{\chi}_j$ is the main decay mode for most cases.

In order to further show the difference between a doublet dominated h_2 and a singlet dominated h_2 , we plot the rate of the $\bar{\tau}\tau$ signal induced by the process $gg \rightarrow h_2 \rightarrow \bar{\tau}\tau$ at 8-TeV LHC with the same samples as those in Fig.6 and Fig.7 respectively. For comparison,

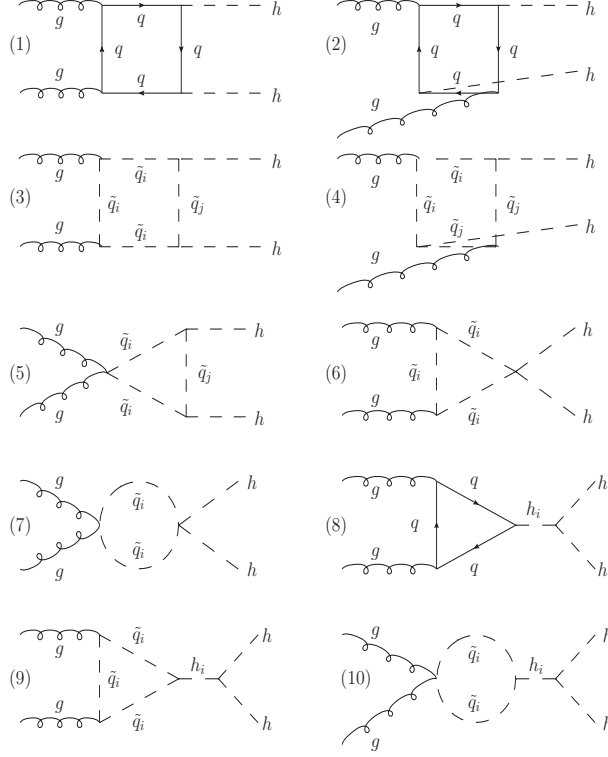


FIG. 9: Feynman diagrams for the pair production of the SM-like Higgs boson via gluon fusion in λ -SUSY with h_i denoting a CP-even Higgs ($i = 1, 2, 3$) and $\tilde{q}_{i,j}$ ($i, j = 1, 2$) denoting a squark. The diagrams with initial gluons or final Higgs bosons interchanged are not shown here. For the quarks and squarks we only consider the third generation due to their large Yukawa couplings.

we also show the direct search bound on this signal from the recent ATLAS analysis. This figure indicates that, for a given m_{h_2} , the $\bar{\tau}\tau$ signal rate induced by a doublet dominated h_2 is usually two order larger than that by a singlet dominated h_2 with same mass. In either case, the rate is at least one order lower than the direct search bound, which means that indirect experimental constraints such as $B \rightarrow X_s \gamma$, the dark matter direct search result and the Higgs data play an important role in deciding the lower mass bound of h_2 .

IV. HIGGS PAIR PRODUCTION AT THE LHC

After the discovery of the Higgs boson, the next important task of the LHC is to reconstruct the Higgs potential and finally decipher the mechanism of the electroweak symmetry breaking. In this direction, the Higgs pair production plays an unique role since it involves the Higgs self interactions. So although the production is a rare process in comparison with

other Higgs processes, it has been paid particular attention in last twenty years[36–38].

In the SM the Higgs pair production at the LHC proceeds by the parton process $gg \rightarrow hh$ through the heavy quark induced box diagrams and also through the production of an off-shell Higgs which subsequently splits into two on-shell Higgs bosons (see diagram (1), (2) and (8) of Fig.9) [36]. The production rate is rather low for $\sqrt{s} = 14\text{TeV}$, about 20 fb at leading order [37] and reaching roughly 35 fb after including the next-to-leading order QCD correction [38]. The capability of the LHC to detect this production process was investigated in [39–42] by the channel such as $gg \rightarrow hh \rightarrow b\bar{b}\gamma\gamma, b\bar{b}WW^*, b\bar{b}\tau^+\tau^-$ respectively, and it has been shown that the most efficient one is $gg \rightarrow hh \rightarrow b\bar{b}\gamma\gamma$ with 6 signal events over 14 background events expected for 600fb^{-1} integrated luminosity after considering some elaborate cuts [39]. In principle, the capability can be further improved if the recently developed jet substructure technique is applied for the Higgs tagging [43].

In SUSY the Higgs pair production may also proceed through the diagrams 3-10 in Fig.9 with the internal particles in the loops involving the third generation squarks and the mediating s-channel scalar involving all CP-even Higgs bosons [44, 45]. Since the genuine SUSY contribution to the amplitude is of the same perturbation order as the SM contribution, the SUSY prediction on the production rate may significantly deviate from the SM result. Based on previous studies in this field[23, 45, 47], we learn that there are three main mechanisms to enhance the production rate greatly:

- Through the loops mediated by stops[45]. In SUSY, the coupling strength of the $h\tilde{t}_i^*\tilde{t}_j$ interaction is mainly determined by the trilinear soft breaking parameter A_t , and consequently, stops contribute to the pair production in following way[45]

$$\mathcal{M} \sim \alpha_s^2 Y_t^2 (c_1 \sin^2 2\theta_t \frac{A_t^2}{m_{\tilde{t}_1}^2} + c_2 \frac{A_t^2}{m_{\tilde{t}_2}^2}), \quad (19)$$

where \mathcal{M} denotes the amplitude of the stop-induced box diagram contribution, Y_t is top quark Yukawa coupling, θ_t is the mixing angle of stops and c_1, c_2 are dimensionless coefficients determined by detailed loop calculation. It is then obvious that the stop contributions may enhance the pair production rate greatly for a light stop together with a large A_t . Detailed calculation indicates that the corrected cross section may be several times larger than its SM prediction[45].

- Through the resonant effect of h_i [23]. In SUSY, h_i may be on-shell produced by gg or $b\bar{b}$ initial state. For $260\text{GeV} \lesssim m_{h_i} \lesssim 400\text{GeV}$, the production rate is not suppressed

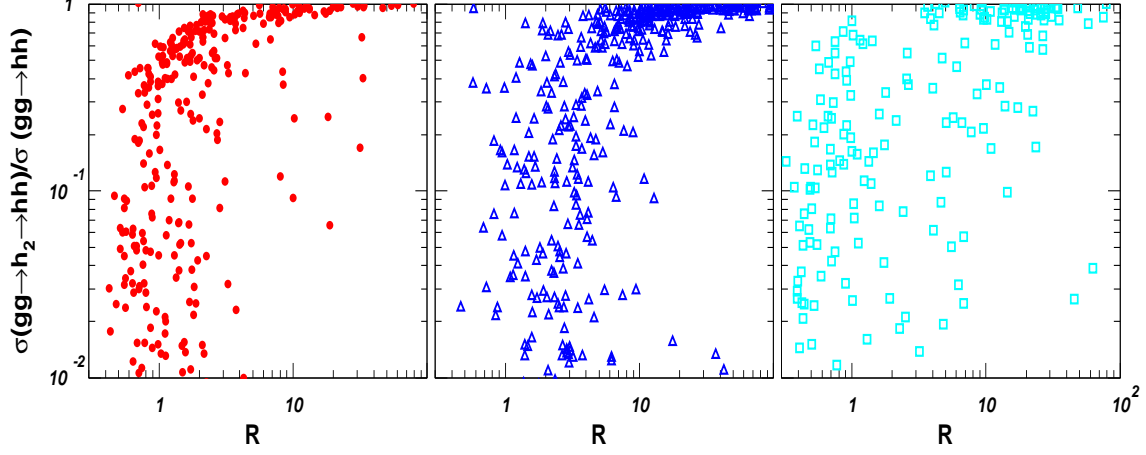


FIG. 10: Correlation between the normalized total cross section $\sigma(pp \rightarrow hh)$, R , and the pure resonant s -channel contribution to the pair production. Results shown in left panel, middle panel and right panel are for Type-I samples, Type-II samples and Type-III samples respectively.

by parton distribution function, and meanwhile h_i may decay dominantly into hh . In this case, the on-shell production of h_i can greatly enhance the pair production rate.

In λ -SUSY, usually only the non-SM doublet dominant h_2 is pertinent to the enhancement, and its resonance effect on the pair production can be estimated by

$$\sigma(gg \rightarrow hh)(pb) \simeq (12.5 \sim 14.5) \times (\cot \beta - \tan \beta A_{\frac{1}{2}}(\tau_b)/A_{\frac{1}{2}}(\tau_t))^2 \times Br(h_2 \rightarrow hh),$$

where $\tau_b = m_{h_2}^2/(4m_b^2)$ and $\tau_t = m_{h_2}^2/(4m_t^2)$. In getting this estimation, we use the fact that $\sigma(gg \rightarrow h_2)$ is about 14.5pb (12.5pb) for $m_{h_2} = 260\text{GeV}$ (350GeV) given that the h_2 has same couplings as the SM Higgs boson to top and bottom quarks[46], and neglect the squark contribution to the $h_2 gg$ coupling. For $\tan \beta = 2$ and $Br(h_2 \rightarrow hh) = 60\%$, one can conclude that the rate is about (1.8 ~ 2.2)pb, which is about 100 times larger than the SM prediction.

- Through large Higgs self coupling[47]. In the SM, the triple self coupling of the Higgs boson plays a minor role in contributing to the pair production due to its relative smallness: $C_{hhh}^{SM} \simeq 32\text{GeV}$, and its effect is to cancel the dominant top quark contribution. While if the self coupling is sufficiently enhanced, the situation will change and the self coupling contribution may become dominant. Given h has same couplings as the SM Higgs boson to top and bottom quarks, and meanwhile neglecting the squark

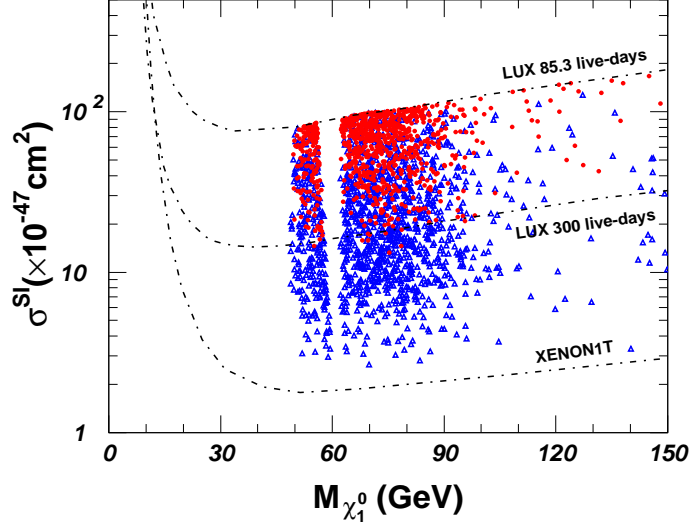


FIG. 11: Same as Fig. 10, but showing the spin-independent χ_1^0 –nucleon scattering cross section as a function of the dark matter only for Type-I and Type-II samples.

contribution to the production, one can estimate the pair production rate by[47]

$$\sigma(gg \rightarrow h^* \rightarrow hh)(pb) \simeq (C_{hhh}/SM - 2.5)^2/1.5^2 \times 0.019, \quad (20)$$

where C_{hhh}/SM is the normalized self coupling of the SM-like Higgs boson in λ -SUSY. This estimation roughly coincides with our precise results presented in Table II for the benchmark points P1 and P2.

In the following, we define $R = \sigma(pp \rightarrow hh)/\sigma_{SM}^{LO}(pp \rightarrow hh) \simeq \sigma(pp \rightarrow hh)/(19\text{fb})$ for the convenience to present our results, and use the same code as [45] to calculate the cross section of $pp \rightarrow hh$ in λ -SUSY. In Fig.10, we present the value of R for Type-I samples, Type-II samples and Type-III samples in left-panel, middle panel and right panel respectively. In order to emphasize the resonance h_2 contribution, we also calculate the process $gg \rightarrow h_2 \rightarrow hh$ separately, and present the ratio $\sigma(pp \rightarrow h_2 \rightarrow hh)/\sigma(pp \rightarrow hh)$ in the same figure. This figure indicates, for Type-I and Type-II samples in λ -SUSY, the Higgs pair production rate may get enhanced by more ten times either through the resonance h_2 effect (corresponding to points with the ratio around one in the figure) or through the large self coupling contribution (corresponding to points with the ratio significantly below one). Especially, in some extreme cases the pair production may get enhanced by more than 100 times for the Type-II sample, which seems impossible in the MSSM[45].

Before we end our discussion, we'd like to point that, because the couplings of h_i with dark matter can be enhanced by a large λ [14], the spin-independent cross section for dark

matter scattering off nucleon may be moderately large. In Fig. 11, we show such a rate as a function of the dark matter mass. In calculating the cross section, we use the formula presented in [48] by choosing a rather low f_{Ts} , $f_{Ts} = 0.025$, which represents the strange quark component in nucleon. This figure indicates that, given LUX experiment with 300 live-days data, most of the Type-I samples will be excluded in case that no dark matter signal is observed. Furthermore, if the updated XENON1T does not detect any signal of the dark matter, all samples of λ -SUSY will be excluded. These facts tell us that the dark matter direct experiments in parallel with collider experiment such as the LHC can serve as a powerful tools in testing the framework of λ -SUSY.

V. SUMMARY AND CONCLUSIONS

Since the first hint of the 125GeV Higgs-like particle appeared at the end of 2011, the unnaturality of the MSSM in predicting the Higgs mass and also the absence of SUSY signal at the LHC have motivated more and more interests of the non-minimal realizations of SUSY. This revived the λ -SUSY theory, which corresponds to the NMSSM with a large λ around one. In the framework of the λ -SUSY, the Higgs mass can be around 125GeV even without the large top-squark radiative correction, and meanwhile the sensitivity of the weak scale to stop masses is reduced by a factor of $(g/\lambda)^2$ in comparison with the MSSM, which means that the lower bound on the stop mass imposed by the LHC direct searches has a weaker implication on fine-tuning in this model than in the MSSM or the NMSSM with a low λ . Due to these advantages, the λ -SUSY has been considered as a most natural realization of SUSY[15, 16].

In order to implement the constraints on the λ -SUSY in a better way, we consider the Higgs data recently updated by the ATLAS and CMS collaborations, for which the consistency of the two group results has been improved greatly. We also define two quantities to measure the naturalness of the parameter points. After these preparations, we scan the parameter space of the λ -SUSY by considering various constraints, then investigate the features of its Higgs sector in physical parameter region. As is shown in this work, the improvement of the two constraints is really necessary. For example, we find the values of the Higgs χ^2 obtained with the latest Higgs data are significantly reduced than before, and the naturalness argument does play an important role in selecting the parameter space of

the λ -SUSY.

For the SM-like Higgs boson h , we have following conclusions:

- Current Higgs data still allow for a sizable singlet component in h , which at most reaches 25%, while the non-SM doublet component is forbidden to be larger than 1%.
- Due the latest Higgs data, the normalized couplings such as $C_{h\gamma\gamma}/SM$, C_{hZZ}/SM and $C_{h\bar{t}t}/SM$ are limited within 10% deviation from unity at 95% C.L.. Compared with the similar fit results in 2012, the optimal values of the couplings in the new fit are shifted significantly.
- Interestingly, the strength of the triple self coupling of h may get enhanced by a factor over 10, and naturalness is capable to put an upper bound on such a coupling.

For the next-to-lightest CP-even Higgs boson h_2 , we find

- For $m_{h_2} \leq 500\text{GeV}$, h_2 is highly non-SM doublet dominated or highly singlet dominated. This feature enables us to express the couplings of h_2 in a simple analytic way.
- For the non-SM double dominated h_2 , it may be as light as 200GeV, which seems impossible in the MSSM. As for its coupling, we find $|C_{h\bar{t}t}/SM| \geq 0.2$, and in optimal case, the normalized coupling is just slightly below 1. On the other hand, $|C_{h\bar{b}b}/SM|$ is usually larger than one with its maximum value reaching 6. In this case, the $h_2 gg$ coupling may be comparable with the SM hgg coupling given a low $\tan\beta$.
- For the singlet dominated h_2 , although it may be as light as 150GeV, its couplings with SM fermions is usually rather weak, so is of less interest in phenomenology study.
- For either the doublet dominated h_2 or the singlet dominated h_2 , the strength of the $h_2 hh$ interaction can be quite large. As a result, $h_2 \rightarrow hh$ may act as the dominant decay channel of h_2 .
- Naturalness disfavors a h_2 with mass at several TeV regardless its field components.

We also investigate the h pair production process, and we find three mechanisms to enhance the rate greatly, i.e. by stop-induced box diagrams, by s-channel resonant h_2 effect

and by large self coupling of h . With these mechanisms, we conclude that the h pair production rate in λ -SUSY may be enhanced by more than 100 times compared with its SM prediction.

In summary, in this work we obtained two characteristic features of λ -SUSY in the experimentally allowed parameter space: 1) the triple self coupling of the SM-like Higgs boson may get enhanced by a factor over 10 in comparison with its SM prediction; 2) the pair production of the SM-like Higgs boson at the LHC may be two orders larger than its SM prediction. These two features seems to be unachievable in the MSSM and in the NMSSM with a low λ , and should be tested at the future LHC.

Acknowledgement

We thank Jinmin Yang, C.-P. Yuan, Haijing Zhou and Jingya Zhu for helpful discussions. This work was supported by the National Natural Science Foundation of China (NNSFC) under grant No. 11222548 and 11275245.

-
- [1] G. Aad *et al.* [ATLAS Collaboration], Phys. Lett. B **716**, 1 (2012) [arXiv:1207.7214 [hep-ex]].
 - [2] S. Chatrchyan *et al.* [CMS Collaboration], Phys. Lett. B **716**, 30 (2012) [arXiv:1207.7235 [hep-ex]].
 - [3] G. Aad *et al.* [ATLAS Collaboration], ATLAS-CONF-2013-034.
 - [4] S. Chatrchyan *et al.* [CMS Collaboration], CMS-PAS-HIG-13-005.
 - [5] G. Aad *et al.* [ATLAS Collaboration], arXiv:1408.7084 [hep-ex].
 - [6] G. Aad *et al.* [ATLAS Collaboration], arXiv:1408.5191 [hep-ex].
 - [7] G. Aad *et al.* [ATLAS Collaboration], ATL-PHYS-PUB-2014-009.
 - [8] S. Chatrchyan *et al.* [CMS Collaboration], CMS-PAS-HIG-14-009.
 - [9] For MSSM explanation of the 125 GeV scalar, see for example
H. Baer, V. Barger and A. Mustafayev, Phys. Rev. D **85**, 075010 (2012) [arXiv:1112.3017 [hep-ph]];
S. Heinemeyer, O. Stal and G. Weiglein, Phys. Lett. B **710**, 201 (2012);
A. Arbey *et al.*, Phys. Lett. B **708**, 162 (2012);

- P. Draper *et al.*, Phys. Rev. D **85**, 095007 (2012);
- M. Carena, *et al.*, JHEP **1203**, 014 (2012);
- S. Akula, *et al.*, Phys. Rev. D **85**, 075001 (2012) [arXiv:1112.3645 [hep-ph]];
- M. Kadastik, *et al.*, JHEP **1205**, 061 (2012) [arXiv:1112.3647 [hep-ph]];
- J. Cao, *et al.*, Phys. Lett. B **710**, 665 (2012) [arXiv:1112.4391 [hep-ph]];
- Z. Kang *et al.*, Phys. Rev. D **86**, 095020 (2012).
- N. D. Christensen, T. Han and S. Su, Phys. Rev. D **85**, 115018 (2012) [arXiv:1203.3207 [hep-ph]];
- H. An, T. Liu and L. T. Wang, Phys. Rev. D **86**, 075030 (2012) [arXiv:1207.2473 [hep-ph]].
- [10] For NMSSM explanation of the 125 GeV scalar, see for example
- U. Ellwanger, JHEP **1203**, 044 (2012) [arXiv:1112.3548 [hep-ph]];
- J. F. Gunion, Y. Jiang and S. Kraml, Phys. Lett. B **710**, 454 (2012) [arXiv:1201.0982 [hep-ph]];
- S. F. King, M. Muhlleitner and R. Nevzorov, Nucl. Phys. B **860**, 207 (2012) [arXiv:1201.2671 [hep-ph]];
- J. J. Cao, *et al.*, JHEP **1203**, 086 (2012) [arXiv:1202.5821 [hep-ph]];
- D. A. Vasquez, *et al.*, Phys. Rev. D **86**, 035023 (2012) [arXiv:1203.3446 [hep-ph]];
- K. Schmidt-Hoberg and F. Staub, JHEP **1210**, 195 (2012) [arXiv:1208.1683 [hep-ph]].
- R. Benbrik, *et al.*, Eur. Phys. J. C **72**, 2171 (2012) [arXiv:1207.1096 [hep-ph]]
- G. Belanger, *et al.*, JHEP **1301**, 069 (2013) [arXiv:1210.1976 [hep-ph]];
- K. Choi, *et al.*, JHEP **1302**, 090 (2013) [arXiv:1211.0875 [hep-ph]];
- S. F. King, *et al.*, Nucl. Phys. B **870**, 323 (2013) [arXiv:1211.5074 [hep-ph]];
- N. D. Christensen, *et al.*, JHEP **1308**, 019 (2013) [arXiv:1303.2113, arXiv:1303.2113 [hep-ph]];
- M. Badziak, M. Olechowski and S. Pokorski, JHEP **1306**, 043 (2013) [arXiv:1304.5437 [hep-ph]];
- S. Moretti, S. Munir and P. Poulose, Phys. Rev. D **89**, 015022 (2014) [arXiv:1305.0166 [hep-ph]];
- W. Wang, J. M. Yang and L. L. You, JHEP **1307**, 158 (2013) [arXiv:1303.6465 [hep-ph]].
- [11] J. Cao, *et al.*, JHEP **1210**, 079 (2012) [arXiv:1207.3698 [hep-ph]].
- [12] P. Bechtle, *et al.*, Eur. Phys. J. C **73**, 2354 (2013) [arXiv:1211.1955 [hep-ph]].
- [13] Z. Kang, J. Li and T. Li, JHEP **1211**, 024 (2012) [arXiv:1201.5305 [hep-ph]].
- [14] U. Ellwanger, C. Hugonie and A. M. Teixeira, Phys. Rept. **496**, 1 (2010); M. Maniatis, Int. J.

- Mod. Phys. A25 (2010) 3505; S. F. King, P. L. White, Phys. Rev. D **52**, 4183 (1995).
- [15] L. J. Hall, D. Pinner and J. T. Ruderman, JHEP **1204**, 131 (2012) [arXiv:1112.2703 [hep-ph]];
M. Perelstein and B. Shakya, Phys. Rev. D **88**, no. 7, 075003 (2013) [arXiv:1208.0833 [hep-ph]];
K. Agashe, Y. Cui and R. Franceschini, JHEP **1302**, 031 (2013) [arXiv:1209.2115 [hep-ph]];
T. Gherghetta, B. von Harling, A. D. Medina and M. A. Schmidt, JHEP **1302**, 032 (2013) [arXiv:1212.5243 [hep-ph]].
- [16] R. Barbieri, D. Buttazzo, K. Kannike, F. Sala and A. Tesi, Phys. Rev. D **87**, no. 11, 115018 (2013) [arXiv:1304.3670 [hep-ph]].
- [17] M. Farina, M. Perelstein and B. Shakya, JHEP **1404**, 108 (2014) [arXiv:1310.0459 [hep-ph]].
- [18] R. Harnik, G. D. Kribs, D. T. Larson and H. Murayama, Phys. Rev. D **70**, 015002 (2004) [hep-ph/0311349];
S. Chang, C. Kilic and R. Mahbubani, Phys. Rev. D **71**, 015003 (2005) [hep-ph/0405267];
R. Barbieri, L. J. Hall, A. Y. Papaioannou, D. Pappadopulo and V. S. Rychkov, JHEP **0803**, 005 (2008) [arXiv:0712.2903 [hep-ph]];
E. Hardy, J. March-Russell and J. Unwin, JHEP **1210**, 072 (2012) [arXiv:1207.1435 [hep-ph]].
- [19] R. Barbieri, L. J. Hall, Y. Nomura and V. S. Rychkov, Phys. Rev. D **75**, 035007 (2007) [hep-ph/0607332].
- [20] J. Cao and J. M. Yang, Phys. Rev. D **78**, 115001 (2008) [arXiv:0810.0989 [hep-ph]].
- [21] A. Djouadi and J. Quevillon, JHEP **1310**, 028 (2013) [arXiv:1304.1787 [hep-ph]].
- [22] ATLAS Collaboration, ATLAS-CONF-2014-049; CMS Collaboration, CMS-PAS-HIG-13-021.
- [23] J. Liu, X. P. Wang and S. h. Zhu, arXiv:1310.3634 [hep-ph];
J. M. No and M. Ramsey-Musolf, Phys. Rev. D **89**, 095031 (2014) [arXiv:1310.6035 [hep-ph]];
B. Bhattacharjee and A. Choudhury, arXiv:1407.6866 [hep-ph].
V. Barger, L. L. Everett, C. B. Jackson, A. Peterson and G. Shaughnessy, arXiv:1408.0003 [hep-ph].
- [24] U. Ellwanger, G. Espitalier-Noel and C. Hugonie, JHEP **1109**, 105 (2011) [arXiv:1107.2472 [hep-ph]].
- [25] U. Ellwanger and C. Hugonie, Comput. Phys. Commun. **175**, 290 (2006); U. Ellwanger, J. F. Gunion and C. Hugonie, JHEP **0502**, 066 (2005).
- [26] The ATLAS collaboration ATLAS-CONF-2013-001; The ATLAS Collaboration CMS-PAS-

SUS-12-023.

- [27] J. Cao, *et al.*, JHEP **1211**, 039 (2012) [arXiv:1206.3865 [hep-ph]];
X. J. Bi, Q. S. Yan and P. F. Yin, Phys. Rev. D **87**, no. 3, 035007 (2013) [arXiv:1209.2703 [hep-ph]];
C. Han, K. i. Hikasa, L. Wu, J. M. Yang and Y. Zhang, JHEP **1310**, 216 (2013) [arXiv:1308.5307 [hep-ph]].
- [28] P. Bechtle, O. Brein, S. Heinemeyer, G. Weiglein and K. E. Williams, Comput. Phys. Commun. **181**, 138 (2010) [arXiv:0811.4169 [hep-ph]];
P. Bechtle, O. Brein, S. Heinemeyer, G. Weiglein and K. E. Williams, Comput. Phys. Commun. **182**, 2605 (2011) [arXiv:1102.1898 [hep-ph]];
P. Bechtle, S. Heinemeyer, O. Stål, T. Stefaniak and G. Weiglein, Eur. Phys. J. C **74**, 2711 (2014) [arXiv:1305.1933 [hep-ph]].
- [29] T. Aaltonen *et al.* [CDF and D0 Collaborations], Phys. Rev. D **88**, no. 5, 052014 (2013) [arXiv:1303.6346 [hep-ex]].
- [30] J. R. Espinosa, C. Grojean, M. Muhlleitner and M. Trott, JHEP **1205**, 097 (2012) [arXiv:1202.3697 [hep-ph]];
P. P. Giardino, K. Kannike, M. Raidal and A. Strumia, JHEP **1206**, 117 (2012) [arXiv:1203.4254 [hep-ph]].
- [31] G. Belanger, B. Dumont, U. Ellwanger, J. F. Gunion and S. Kraml, JHEP **1302**, 053 (2013) [arXiv:1212.5244 [hep-ph]];
F. Boudjema, *et al.*, arXiv:1307.5865 [hep-ph].
- [32] J. Cao, F. Ding, C. Han, J. M. Yang and J. Zhu, JHEP **1311**, 018 (2013) [arXiv:1309.4939 [hep-ph]].
- [33] A. Djouadi, Phys. Rept. **459**, 1 (2008) [hep-ph/0503173].
- [34] A. Arbey, M. Battaglia and F. Mahmoudi, Phys. Rev. D **88**, no. 1, 015007 (2013) [arXiv:1303.7450 [hep-ph]].
- [35] K. J. Bae, H. Baer, V. Barger, D. Mickelson and M. Savoy, arXiv:1407.3853 [hep-ph].
- [36] E. W. N. Glover and J. J. van der Bij, Nucl. Phys. B **309**, 282 (1988).
D. A. Dicus, C. Kao and S. S. D. Willenbrock, Phys. Lett. B **203**, 457 (1988).
T. Plehn, M. Spira and P. M. Zerwas, Nucl. Phys. B **479**, 46 (1996) [Erratum-ibid. B **531**, 655 (1998)] [hep-ph/9603205].

- [37] A. Djouadi, W. Kilian, M. Muhlleitner and P. M. Zerwas, Eur. Phys. J. C **10**, 45 (1999) [hep-ph/9904287].
- [38] J. Baglio, A. Djouadi, R. Grober, M. M. Muhlleitner, J. Quevillon and M. Spira, JHEP **1304**, 151 (2013) [arXiv:1212.5581 [hep-ph]].
D. Y. Shao, C. S. Li, H. T. Li and J. Wang, JHEP **1307**, 169 (2013) [arXiv:1301.1245 [hep-ph]];
D. de Florian and J. Mazzitelli, Phys. Lett. B **724**, 306 (2013) [arXiv:1305.5206 [hep-ph]];
J. Grigo, J. Hoff, K. Melnikov and M. Steinhauser, Nucl. Phys. B **875**, 1 (2013) [arXiv:1305.7340 [hep-ph]];
D. de Florian and J. Mazzitelli, Phys. Rev. Lett. **111**, 201801 (2013) [arXiv:1309.6594 [hep-ph]];
R. Frederix, S. Frixione, V. Hirschi, F. Maltoni, O. Mattelaer, P. Torrielli, E. Vryonidou and M. Zaro, Phys. Lett. B **732**, 142 (2014) [arXiv:1401.7340 [hep-ph]];
L. Liu-Sheng, Z. Ren-You, M. Wen-Gan, G. Lei, L. Wei-Hua and L. Xiao-Zhou, Phys. Rev. D **89**, 073001 (2014) [arXiv:1401.7754 [hep-ph]];
J. Grigo, K. Melnikov and M. Steinhauser, arXiv:1408.2422 [hep-ph].
- [39] U. Baur, T. Plehn and D. L. Rainwater, Phys. Rev. D **69**, 053004 (2004) [hep-ph/0310056];
W. Yao, arXiv:1308.6302 [hep-ph];
V. Barger, L. L. Everett, C. B. Jackson and G. Shaughnessy, Phys. Lett. B **728**, 433 (2014) [arXiv:1311.2931 [hep-ph]];
G. Aad *et al.* [ATLAS Collaboration], arXiv:1406.5053 [hep-ex].
- [40] A. Papaefstathiou, L. L. Yang and J. Zurita, Phys. Rev. D **87**, 011301 (2013) [arXiv:1209.1489 [hep-ph]].
F. Goertz, A. Papaefstathiou, L. L. Yang and J. Zurita, JHEP **1306**, 016 (2013) [arXiv:1301.3492 [hep-ph]].
- [41] M. J. Dolan, C. Englert and M. Spannowsky, JHEP **1210**, 112 (2012) [arXiv:1206.5001 [hep-ph]].
- [42] N. D. Christensen, T. Han and T. Li, Phys. Rev. D **86**, 074003 (2012) [arXiv:1206.5816 [hep-ph]].
R. Contino, M. Ghezzi, M. Moretti, G. Panico, F. Piccinini and A. Wulzer, JHEP **1208**, 154 (2012) [arXiv:1205.5444 [hep-ph]].
Q. Li, Q. S. Yan and X. Zhao, Phys. Rev. D **89**, 033015 (2014) [arXiv:1312.3830 [hep-ph]];

- D. E. Ferreira de Lima, A. Papaefstathiou and M. Spannowsky, JHEP **1408**, 030 (2014) [arXiv:1404.7139 [hep-ph]].
- [43] J. M. Butterworth, A. R. Davison, M. Rubin and G. P. Salam, Phys. Rev. Lett. **100**, 242001 (2008) [arXiv:0802.2470 [hep-ph]];
M. Gouzevitch, A. Oliveira, J. Rojo, R. Rosenfeld, G. P. Salam and V. Sanz, JHEP **1307**, 148 (2013) [arXiv:1303.6636 [hep-ph]];
A. J. Barr, M. J. Dolan, C. Englert and M. Spannowsky, Phys. Lett. B **728**, 308 (2014) [arXiv:1309.6318 [hep-ph]].
- [44] S. H. Zhu, C. S. Li and C. S. Gao, Phys. Rev. D **58**, 015006 (1998);
A. Belyaev, M. Drees and J. K. Mizukoshi, Eur. Phys. J. C **17**, 337 (2000);
C. S. Kim, K. Y. Lee and J. -H. Song, Phys. Rev. D **64**, 015009 (2001);
D. T. Nhung, M. Muhlleitner, J. Streicher and K. Walz, JHEP **1311**, 181 (2013) [arXiv:1306.3926 [hep-ph]];
U. Ellwanger, JHEP **1308**, 077 (2013) [arXiv:1306.5541, arXiv:1306.5541 [hep-ph]];
C. Han, X. Ji, L. Wu, P. Wu and J. M. Yang, JHEP **1404**, 003 (2014) [arXiv:1307.3790 [hep-ph]].
- [45] J. Cao, Z. Heng, L. Shang, P. Wan and J. M. Yang, JHEP **1304**, 134 (2013) [arXiv:1301.6437 [hep-ph]].
- [46] See for example, <https://twiki.cern.ch/twiki/bin/view/LHCPhysics/CrossSections>.
- [47] J. Cao, Y. He, P. Wu, M. Zhang and J. Zhu, JHEP **1401**, 150 (2014) [arXiv:1311.6661 [hep-ph]].
- [48] J. Cao, K. -i. Hikasa, W. Wang, J. M. Yang and L. -X. Yu, JHEP **1007**, 044 (2010) [arXiv:1005.0761 [hep-ph]].
- [49] D. S. Akerib *et al.* [LUX Collaboration], Phys. Rev. Lett. **112**, 091303 (2014) [arXiv:1310.8214 [astro-ph.CO]].
- [50] After neglecting gauge interactions, the coupling of h_2 with dark matter is determined by terms $\lambda \hat{H}_u \cdot \hat{H}_d \hat{S} + \frac{1}{3} \kappa \hat{S}^3$ in the superpotential. For a singlet dominated h_2 , the coupling strength is mainly determined by λ for bino-like dark matter and by κ for singlino-like dark matter. Given the potentially largeness of λ and κ , the strength is moderately large. While for a doublet dominated h_2 , only its coupling with bino-like dark matter is sizable, and it is significantly smaller than the similar coupling for a singlet dominated h_2 because there is no

bino-singlino mixing in neutralino mass matrix.